Approximate Large-Signal Analysis of IMPATT Oscillators

By J. L. BLUE

(Manuscript received August 11, 1968)

Insight into the large-signal operating characteristics of IMPATT oscillators has been obtained from detailed numerical calculations of D. L. Scharfetter and H. K. Gummel. However, their calculations are relatively expensive in computer time. Small-signal analyses of IMPATT diodes are much less expensive, but give little reliable information about oscillator performance.

This paper presents a model for large-signal analysis of IMPATT diodes which requires less than 1 percent of the computer time used by Scharfetter and Gummel's method, but still provides a realistic description of IMPATT oscillators in modes of operation which maintain carrier velocity saturation. We show graphical results, based on numerical computations, which provide information about phase relationships in IMPATT oscillators and improve understanding of the two-frequency mode of operation.

I. INTRODUCTION

Considerable insight into the large-signal operating characteristics of IMPATT oscillators has recently been obtained by D. L. Scharfetter and H. K. Gummel through numerical calculations involving a complete modeling of the physical processes taking place in the diode.[1] They solve the one-dimensional partial differential equations for the generation, diffusion, and drift of holes and electrons, as well as Poisson's equation and the differential equations for the circuit in which the diode is embedded. Their analysis, which has led to improved understanding of IMPATT diodes and insight into new modes of oscillation, includes most of the important physical effects. Since their model is so detailed and accurate, their analysis is a large-scale computer project. Even after the computer programs are debugged, analysis of IMPATT diodes is relatively expensive.

Another possible method is small-signal analysis, which is tractable numerically and more economical.[2–4] However, small-signal analysis gives only a limited amount of information about large-signal oscillation.

An intermediate model has been presented by W. J. Evans.[5] However, his simplified large-signal model requires short transit-time in the drift region. He obtained a single first-order differential equation for the diode current, and was able to solve analytically for the (large-signal) diode current and voltage as a function of time. Unfortunately, the restriction to short transit time and bis use of other approximations severely limit the applicability of his results.

This paper presents a model for large-signal analysis of IMPATT diodes which incorporates most of tbe important physical processes in the diodes, but which is more tractable numerically than that of Scharfetter and Gummel. Because the new model requires far fewer computer hours than Scharfetter and Gummel's model, parameter studies are feasible; because the new model contains more physics than Evans' model or tbe small-signal models, the results are more reliable and more effects can be studied.

II. LARGE-SIGNAL IMPATT MODEL

We consider a one-dimensional diode, neglect diffusion, and assume that the electric field is large enough so that holes and electrons move at scatter-limited velocities. The latter assumption is essential for simplifying the calculations, but means that our model is not applicable to some important oscillator modes, such as analyzed by Scharfetter, Bartelink, and Johnston.[6]

The other important simplification is that in Poisson's equation we neglect the space charge of the ac component of the particle current in the avalanche region. The detailed calculations of Scharfetter and Gummel show that this is a good approximation for tbe classical Read mode of operation and other modes where the width of the avalanche region remains fairly constant during tbe oscillation cycle.[7] We include the space charge of the dc component of the particle current in the avalanche region, and both ac and dc components of the particle current in the drift region. This says that tbe sbape of the electric field profile in the avalanche region does not cbange in time, although the magnitude of the field does; that is,

$$E_{aval}(x, t) = f(x) + E(t). \tag{1}$$

This is equivalent to the commonly-made assumption that the particle current is constant in the avalanche region.[2, 5, 7] Given a bias current and the doping in the diode, we can calculate $f(x)$ by solving a second-order differential equation by standard methods.[3, 4]

We can treat diodes in which holes and electrons have unequal scatter-limited velocities and unequal ionization coefficients, although the model we have chosen for computation assumes the same values for electrons as for holes. The ionization coefficients may be any given function of the electric field, such as $A \exp(-b/E)$.

Besides the simplifications resulting from our diode model, we obtain important simplifications by solving directly for a periodic solution, rather than solving for a transient solution which eventually becomes periodic. We save computation time both because we eliminate solving for the unneeded transient solution, and because we are able to use more advantageous numerical methods.

Notice that the essential approximations are constant carrier velocities and equation (1); many combinations of additional approximations may be made, so that we are describing a whole hierarchy of IMPATT models. The aproximation of equation (1) can be overcome by a recursive method of solution, the first step of which is the subject of this paper. However, for most purposes equation (1) is sufficiently accurate.

III. IDEALIZED DIODE

In the rest of this paper, we consider a fairly simple model of an IMPATT diode; we are able to emphasize the essential features of the method without becoming lost in algebra. (We plan to treat the most general case in a subsequent article.)

We consider a diode with a uniform electric field [$f(x) = 1$] in the avalanche region (of length d_a), and one drift region (of length d_d). We assume equal hole and electron velocities and ionization coefficients, so that the continuity equations for holes and electrons in the avalanche region are

$$\partial p(x, t)/\partial t = v\alpha[E(t)][p(x, t) + n(x, t)] - v\, \partial p(x, t)/\partial x$$

$$\partial n(x, t)/\partial t = v\alpha[E(t)][p(x, t) + n(x, t)] + v\, \partial n(x, t)/\partial x.$$

The importance of the approximations discussed in Section II is that they enable us to avoid dealing with the hole and electron densities as functions of both space and time. We proceed much as did

Read[7] and Evans,[5] adding the two continuity equations to obtain an equation involving the particle current density

$$\partial I_p(x, t)/\partial t = 2v\alpha I_p - qv^2\,\partial(p - n)/\partial x. \tag{2}$$

The total current, particle plus displacement, is

$$I_T(t) = I_p(x, t) + \epsilon\,\partial E(x, t)/\partial t. \tag{3}$$

I_T is independent of x; since E in the avalanche region is independent of x, $I_p(x, t)$ is also independent of x. Using this fact, we integrate equation (2) over the avalanche region. Neglecting reverse saturation current, we obtain

$$\partial I_p/\partial t = \frac{2vI_p}{d_a}\{d_a\alpha[E(t)] - 1\}.$$

If we use $\alpha(E) = A\exp(-b/E)$, and define E_c as the "critical" field (that field necessary to maintain the dc current under static conditions) then $\alpha(E_c) = 1/d_a$. We obtain

$$\partial I_p/\partial t = \frac{2vI_p}{d_a}[(Ad_a)^{1-E_c/E(t)} - 1]. \tag{4}$$

(Evans linearized the electric field, and used

$$\partial I_p/\partial t = \frac{2v}{d_a} I_p m\left[\frac{E(t)}{E_c} - 1\right].$$

We retain the more nonlinear version.)

We treat the case in which there is an applied voltage* $V(t)$ in excess of that required to maintain the dc reverse bias current density I_o. The avalanche electric field is reduced by the space charge of the particle current in the drift region; as in Read, we have

$$E(t) = E_c + V(t)/(da + d_d) - \frac{1}{\epsilon}\int_{t-T_d}^{t} I_p(t')\left(1 - \frac{t' - t}{T_d}\right)dt' \tag{5}$$

where $T_d = d_d/v$ is the time for particles to pass through the drift region after leaving the avalanche region. In equation (5) and the remainder of this paper we specialize to the case $d_a \ll d_d$, as Read and Evans did.

Equations (4) and (5), together with suitable initial conditions, may be solved for $E(t)$ and $I_p(t)$. The total current, which is equal

* We could equally well treat the case where there is an applied terminal current $I_T(t)$. It is only slightly more difficult to embed the diode in a circuit; then we use Kirchoff's laws to write $V(t)$ in terms of $I_T(t)$ and the circuit parameters, generally as an integral over I_T.

to the terminal current, may be obtained from equation (3):

$$I_T(t) = \frac{\epsilon}{d_a + d_d} dV(t)/dt + \frac{1}{T_d} \int_{t-T_d}^{t} I_p(t')\, dt'. \tag{6}$$

The first term is the displacement current and the second is the particle-induced terminal current, I_{T_p}.

Instead of solving the initial-value equations for the transient solution, and extending the solution far enough in time for the limiting periodic solution to be obtained, it is preferable to solve directly for only the periodic solution. We assume $V(t)$ to be periodic (not necessarily sinusoidal) with period τ, and find solutions $E(t)$ and $I_p(t)$ which also have period τ. Now we need solve only for t in the interval $(0, \tau)$. It is more convenient to rewrite equation (4) as an integral equation; integrating equation (4) from 0 to t, we obtain ($T_a = d_a/v$)

$$I_p(t) = I_p(0) \exp\left\{\frac{2}{T_a} \int_0^t [(Ad_a)^{1-E_c/E(t')} - 1]\, dt'\right\}. \tag{7}$$

We substitute equation (5) for $E(t')$, and bave a single integral equation for $I_p(t)$, which we sball not write explicitly; since $I_p(t + \tau) = I_p(t)$, we solve only for $0 \leqq t \leqq \tau$. Because of its complexity, it will be solved numerically; for our metbod to be useful, we must be able to find numerical solutions quickly and reliably. We solve this nonlinear integral equation by a standard iterative method, which converges quickly and stably.

We divide the interval $(0, \tau)$ into M intervals, let $t_n = n\tau/M$, and solve equation (7) approximately for the M values $I_p(t_n)$, $n = 1, 2, \ldots, M$. The integrals are evaluated by, for example, the trapezoidal rule, with integrands evaluated only at times t_n. We obtain a system of M nonlinear equations for the values $I_p(t_n)$, which are easily solved by, for example, the matrix analog of the Newton-Raphson method. More accurate integration rules than the trapezoidal rule may be used. They are more complicated to program, but save execution time because, for a given accuracy, fewer points need be used.

After the $I_p(t_n)$ are found, then the $I_T(t_n)$ may be found from equation (6). Then we Fourier-analyze I_T and V; the ratio of their fundamental components is the large-signal admittance at the frequency $\nu = 1/\tau$. The ac power delivered by the diode also is easily calculated.

Tbe small-signal admittance can be calculated analytically. It is

$$Y(\omega) = \frac{\epsilon}{(d_a + d_d)T_d} \left[\frac{1 - \omega^2/\omega_a^2}{\xi(\omega) + i\omega/\omega_a^2 T_d}\right]$$

where

$$\xi(\omega) = \frac{\exp(-i\omega T_d) - 1 + i\omega T_d}{(-i\omega T_d)^2}$$

and

$$\omega_a^2 = \frac{2\alpha'(E_c)vI_0}{\epsilon}.$$

This admittance agrees with that of Gilden and Hines, when their "passive resistance of the inactive zone R_s" is neglected.[2]

IV. RESULTS

We analyze a germanium IMPATT oscillator similar to the one reported by Swan.[8] The results, which are presented graphically, are meant more as an illustration of typical results obtainable than as a comprehensive analysis of Swan's oscillator. In particular, the uniform avalanche region approximation is inadequate. However, even these preliminary results can clarify some aspects of IMPATT oscillator operation.

The diode we analyzed has an avalanche width $d_a = 1.5 \times 10^{-4}$ cm, a drift width $d_d = 3.5 \times 10^{-4}$ cm, and a carrier velocity $v = 5 \times 10^6$ cm per second. The ionization coefficient is $\alpha(E) = 5.9 \times 10^{+6}$ cm^{-1} exp[-1.2×10^6 (V/cm)/E].

Figure 1 shows typical solutions for the ac components of $V(t)$, $I_p(t)$, and $I_{T_p}(t)$. Two cycles are shown; we plot I_{T_p} instead of I_T, because the displacement current component of I_T delivers no power. The frequency is 5 GHz, and the ac voltage amplitude is 10 volts. The avalanche region particle current is extremely nonsinusoidal, and becomes more so with increasing ac voltage amplitude. The fundamental component of $I_p(t)$ lags the ac voltage by about 49.5 degrees; this phase angle also increases with increasing ac voltage, approaching 90 degrees. The phase is closer to 90 degrees for higher frequencies; this may be attributed to the lessened effect of drift region space charge on the avalanche region field. (Read showed that the phase is 90 degrees when the space charge can be neglected, so that the electric field in the avalanche region is in phase with the terminal voltage.) The phase will be discussed further in connection with Fig. 3.

Figure 2 is a complex-plane admittance plot; the dc component of I_T is fixed at 500 A/cm^2, and the ac component of $V(t)$ is a pure sine wave, as it would be if the diode were embedded in a high-Q parallel

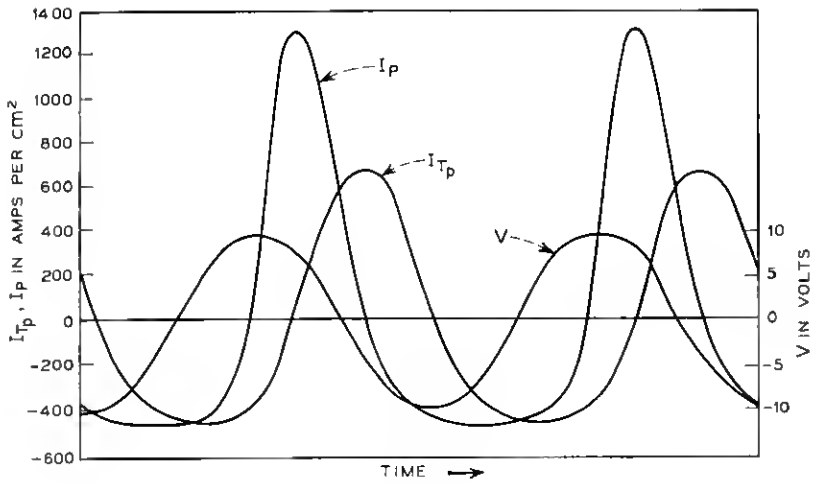

Fig. 1— AC components of V, I_p, I_{T_p} at frequency 5 GHz, current density 500 A/cm², ac voltage amplitude 10 V. Two cycles shown.

resistance-impedance-capacitance (RLC) circuit with only one resonant frequency. The solid curves are curves of constant ac voltage amplitude; the dashed lines are curves of constant frequency. For frequencies about 6 GHz and above, the negative conductance decreases with increasing ac voltage amplitude. For lower frequencies, the negative conductance first increases, then decreases with increasing ac voltage amplitude. For some low frequencies, for example 4 GHz, the diode has positive small-signal conductance, but negative large-signal conductance for large enough ac voltage. This type of behavior agrees with that found at low frequencies by the detailed calculations of Scharfetter and Gummel.[9]

Insight into this type of behavior may be obtained from Fig. 3, which shows the amplitude and phase (with respect to the ac voltage) of the fundamental component of $I_p(t)$. Curves of constant ac voltage amplitude are solid and curves of constant frequency are dashed. To transform any point on this plot to a complex admittance plot, one first multiplies the complex number representing the point by

$$[\exp(-i\omega T_d) - 1]/(-i\omega T_d)$$

to give the fundamental component of I_{T_p}. (For small ωT_d, this is approximately the same as rotating the phase plot point of I_p clockwise

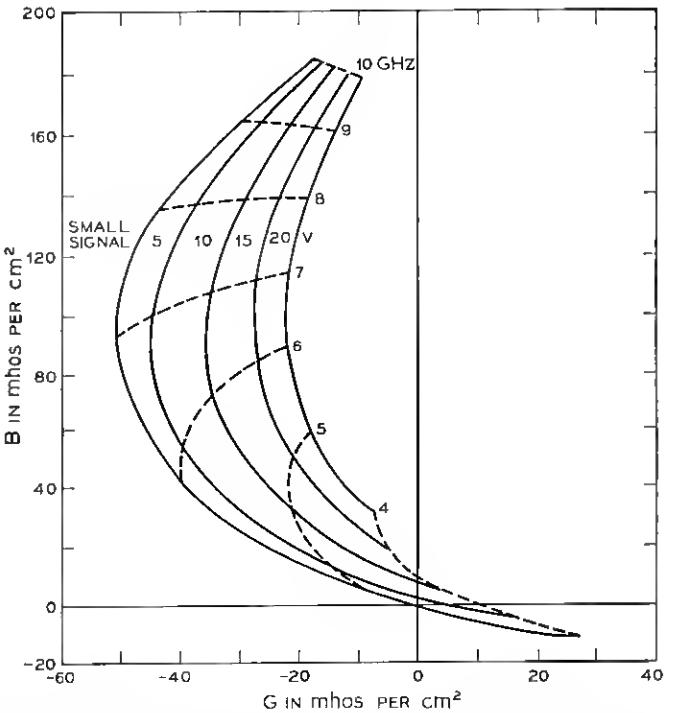

Fig. 2 — Complex-plane plot of diode admittance as a function of frequency and ac voltage amplitude. AC component of $V(t) = A \cos \omega t$. Current density 500 A/cm².

by $\frac{1}{2}\omega T_d$.) If the resulting point is in the second or third quadrant, then the diode has negative conductance at that frequency and ac voltage amplitude. Then the amplitude is divided by the magnitude of the fundamental component of the ac voltage amplitude; finally the point is moved directly upwards by $\epsilon\omega/(d_a + d_d)$ to add in the displacement current component.

At low frequencies, increased ac voltage amplitude improves the avalanche current phase considerably; at 4 GHz, where the small-signal conductance is positive, the improvement is sufficient so that the approximately $\frac{1}{2}\omega T_d$ rotation puts the phase plot point into the third quadrant, and negative conductance results for amplitudes above about 12 volts.

Figure 4 shows output power in the fundamental, in watts per square centimeter. Maximum output power is obtained near the fre-

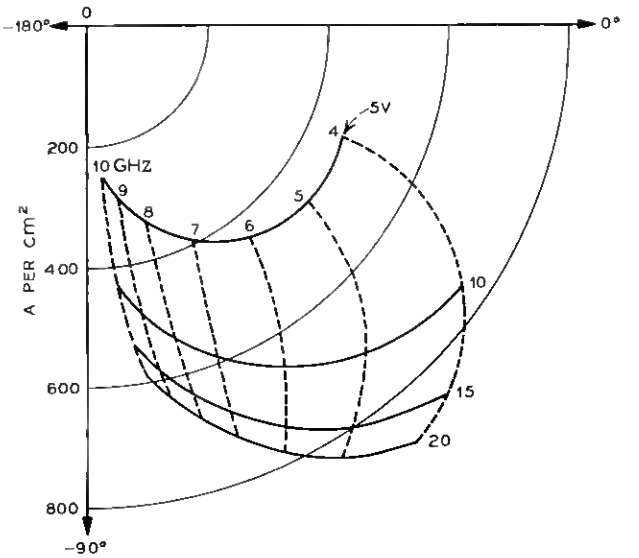

Fig. 3 — Magnitude and phase plot of fundamental component of avalanche particle current, $I_p(t)$, as a function of frequency and ac voltage amplitude. Current density 500 A/cm².

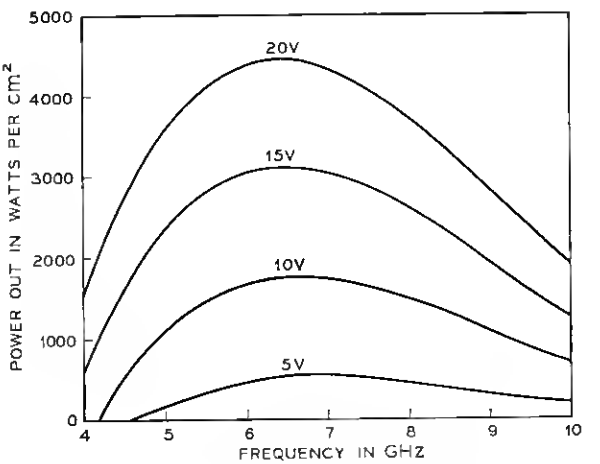

Fig. 4 — Output power vs frequency for various ac voltage amplitudes. Current density 500 A/cm².

quency with largest small-signal negative conductance. Efficiency depends upon the dc voltage across the diode, and therefore on the dc electric field in the drift region. The idealized model merely assumes this field large enough to maintain scatter-limited velocity. A better lower bound is obtained by calculating, at each point in the diode, the reduction in field resulting from the space charge of the current pulse drifting away from the avalanche region. Since I_T is independent of x,

$$\epsilon\, dE(x, t)/dt = I_p(t) + \epsilon\, dE_{aval}(x, t)/dt - I_p(t - x/v).$$

Integrate from 0 to t and subtract the dc component to obtain

$$\Delta E(x, t) = \Delta E_{aval}(t) + \int_0^t [I_p(t') - I_p(t' - x/v)]\, dt'.$$

Requiring the dc field at x to be as least as large as

$$\max_t [-\Delta E(x, t)]$$

gives the minimum field in the drift region allowable, and thus gives the minimum drift voltage and maximum efficiency. The maximum ΔE is also of interest, since in our model it is assumed that no avalanching takes place in the drift region. If E_a is the minimum electric field for which appreciable avalanche ionization can take place, then we must require that

$$\max [\Delta E(x, t)] + \max [-\Delta E(x, t)] < E_a$$

for all x. This limits the allowable ac voltage amplitude. Numerical results indicate that, for a given current density, the allowable ac voltage amplitude depends only weakly on the frequency of oscillation and the shape of the voltage waveform $V(t)$. For our sample diode, if $E_a \approx 10^5$ volt/cm, 20 volts ac amplitude is, approximately, the limiting voltage for the simple diode model used. A more general model, with a nonuniform avalanche region, could partially include avalanche-broadening, and thus be used to analyze diode modes of operation with larger ac voltage amplitudes.

Swan, Lee, and Standley recently reported marked improvement in the performance of an IMPATT oscillator embedded in a microwave circuit resonant at two frequencies, the fundamental and its second harmonic.[8, 10] As an aid in understanding their results, in the rest of this section we present calculations in which $V(t)$ has the form $V_o \cos \omega t + \frac{1}{2} V_o \sin 2\omega t$. (This particular waveform is not the

optimum form, but is illustrative.) "Best" values of the magnitude and phase of the second harmonic depend on the frequency and magnitude of the fundamental, the bias current, the particular diode used, and the standards of performance to be applied to the diode.

Figures 5 to 8 correspond to Figs. 1 to 4; V_o is now chosen so that half the peak-to-peak value of $V(t)$ is 5, 10, 15, or 20 volts. In comparing the oscillations resulting from a two-frequency $V(t)$ with a one-frequency $V(t)$, we have chosen to compare voltage waveforms with equal ac peak-to-peak amplitudes, not with equal amplitudes in the fundamental, because of the ac amplitude limitation discussed earlier.

Figure 5 shows solutions for the ac components of $V(t)$, $I_p(t)$, and $I_{T_p}(t)$; the frequency of the fundamental is 5 GHz, and the maximum ac voltage is 10 volts. The fundamental component of $I_p(t)$ lags the fundamental component of the ac voltage by about 60 degrees instead of 49.5 degrees.

Figure 6 is a complex-plane admittance plot; for clarity, the lines of constant ac voltage are omitted, and dots are placed at 0, 5, 10, 15, and 20 volts. For nonsinusoidal ac voltages, the admittance at the fundamental can move to the left of the small-signal admittance line, resulting in a better negative conductance-to-susceptance ratio. This is especially apparent at 4 GHz; comparison of the 4 GHz, 20

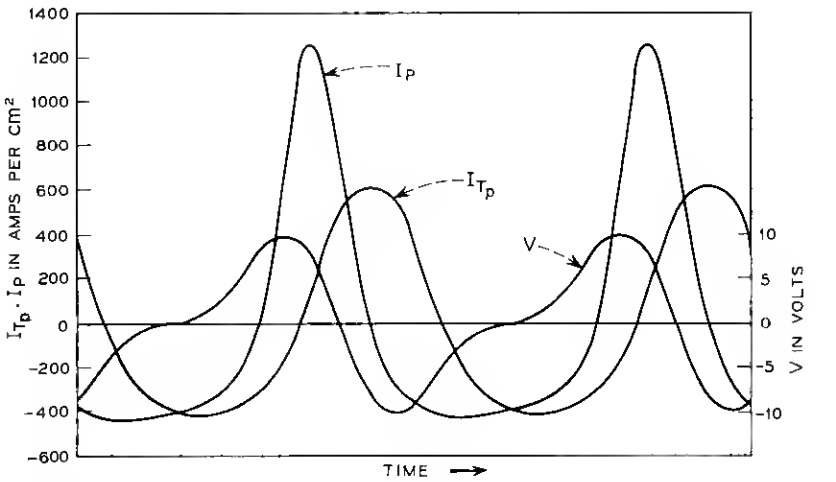

Fig. 5—AC components of V, I_p, I_{T_p} at frequency 5 GHz, current density 500 A/cm², ac voltage amplitude 10 V. Two cycles shown.

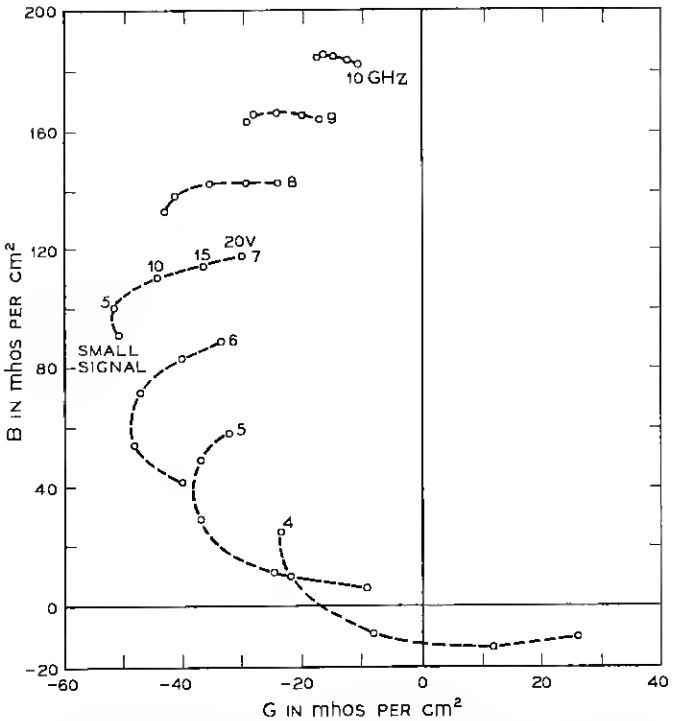

Fig. 6 — Complex-plane plot of diode admittance at fundamental frequency as a function of frequency and maximum ac voltage. AC component of $V(t) = V_a \cos \omega t + \frac{1}{2} V_a \sin 2\omega t$. Current density 500 A/cm².

V points in Figs. 2 and 6 indicates that the addition of a second harmonic component has improved the diode negative conductance by a factor of three, and the negative conductance-to-susceptance ratio by a factor of four.

Figure 7, corresponding to Fig. 3, shows in more detail the phase improvement obtained with addition of the harmonic component to the ac voltage.

Figure 8 shows output power in the fundamental. At higher frequencies, maximum output power is less than that shown in Fig. 4. At 5 GHz, maximum output power is about the same as in Fig. 4, but occurs at an improved negative conductance-to-susceptance ratio. This ratio is important when the diode's parasitic resistance R_p, which we have neglected, is included, since the power is proportional to

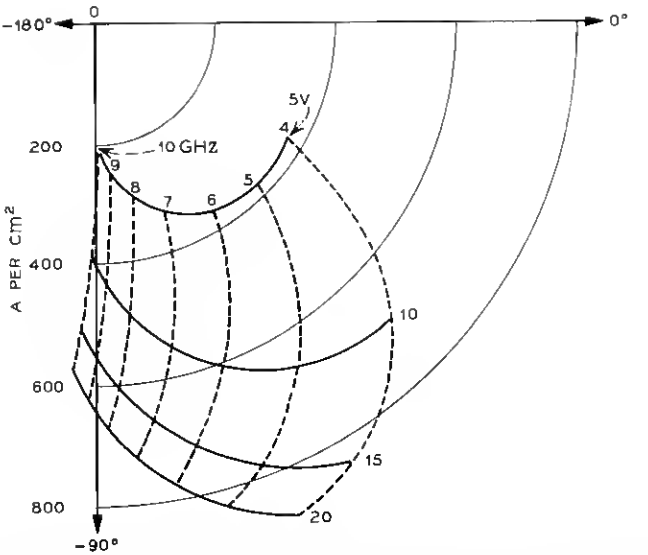

Fig. 7 — Magnitude and phase plot of fundamental component of avalanche particle current, $I_p(t)$, as a function of frequency and ac voltage amplitude. Current density 500 A/cm².

$- G/(G^2 + B^2) - R_p$. At 4 GHz, maximum output power is substantially better than that shown in Fig. 4. The nonsinusoidal form of $V(t)$ improves the phase of $I_T(t)$ sufficiently so that, even though $V(t)$ contains less of the fundamental, the output power in the fundamental remains about the same.

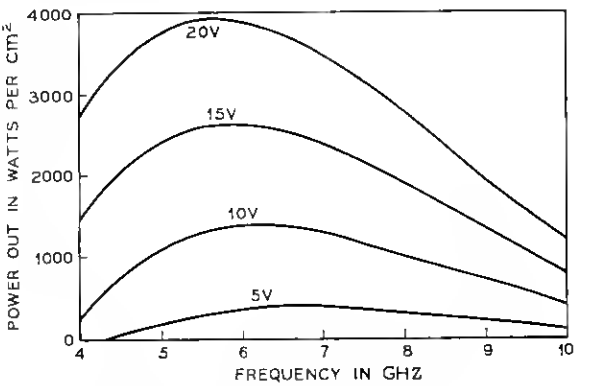

Fig. 8 — Output power in fundamental vs frequency for various maximum ac voltages. Current density 500 A/cm².

V. CONCLUSIONS

We have presented a numerically tractable method for analyzing large-signal IMPATT oscillators. It requires less than 1/100 of the computer time used by Scharfetter and Gummel's method, but still provides a realistic description of IMPATT oscillators in modes of operation which maintain carrier velocity saturation. (One solution takes about one second of computation time on the GE 645 computer, if we use 15 time steps per period.) Numerical calculations based on a simplified version of the model have provided information about the phase relationships in an IMPATT oscillator and improved understanding of the two-frequency mode of operation.

REFERENCES

1. Scharfetter, D. L. and Gummel, H. K., "Large-Signal Analysis of a Silicon Read Diode Oscillator," to be published in IEEE Trans. Elec. Devices, *ED-16*, No. 1 (January 1969).
2. Gilden, M. and Hines, M. B., "Electronic Tuning Effects in the Read Microwave Avalanche Diode," IEEE Trans. Electron Devices, *ED-13*, No. 1 (January 1966), pp. 169–175.
3. Gummel, H. K. and Scharfetter, D. L., "Avalanche Region of IMPATT Diodes," B.S.T.J., *45*, No. 10 (December 1966), pp. 1797–1827.
4. Gummel, H. K. and Blue, J. L., "A Small-Signal Theory of Avalanche Noise in IMPATT Diodes," IEEE Trans. Electron Devices, *ED-14*, No. 9 (September 1967), pp. 569–580.
5. Evans, W. J., "Nonlinear and Frequency Conversion Characteristics of IMPATT Diodes," Technical Report No. 104, Electron Physics Laboratory, Department of Electrical Engineering, The University of Michigan, February 1968. Also see: Evans, W. J., and Haddad, G. I., "A Large-Signal Analysis of IMPATT Diodes," IEEE Trans. Elec. Devices, *ED-15*, No. 10 (October 1968), pp. 708–716.
6. Scharfetter, D. L., Bartelink, D. J., and Johnston, R. L., "High Efficiency Subtransit Time Oscillations in Germanium Avalanche Diodes," Proc. IEEE, *56*, No. 9 (September 1968), pp. 1611–1612.
7. Read, W. T., Jr., "A Proposed High-Frequency, Negative Resistance Diode," B.S.T.J., *37*, No. 3 (March 1958), pp. 401–446.
8. Swan, C. B., "IMPATT Performance Improvement with Second Harmonic Tuning," Proc. IEEE, *56*, No. 9 (September 1968), pp. 1616–1617.
9. Scharfetter, D. L., private communication.
10. Lee, T. P. and Standley, R. D., "Frequency Modulation of a Millimeter-wave IMPATT Diode Oscillator and Related Harmonic Generation Effects," B.S.T.J., *48*, No. 1 (January 1969), pp. 143–161.